æ

8. EVOLUTIONARY SCALING RELATIONSHIPS IN CELL BIOLOGY

14 August 2022

Cells vary widely in terms of shape, physiological properties, metabolic features, and internal architecture. Of particular importance is cell size, which influences a myriad of cellular features ranging from nutrient uptake to internal transport. Cell-size variation among species is likely driven by a variety of selective forces, including size-selective predators, buoyancy, resistance to flow dynamics, and osmotic pressure. Among the most well-studied unicellular species, cell volumes vary by approximately eleven orders of magnitude, 10^{-3} to 10^{8} μm^3, across the Tree of Life, with up to 10^{7}-fold differences within major phylogenetic groups (Figure 8.1). By comparison, the range in size between the smallest and largest mammals, a bumblebee bat vs. a blue whale, is eight orders of magnitude. On average, prokaryotic cells are smaller than those of eukaryotic species, but some eukaryotes have cell volumes smaller than the average bacterium.

There are a few striking exceptions at the large end of the scale not shown in Figure 8.1. For example, the unicellular green alga *Acetabularia* is up to 10 cm in length and contains just a single nucleus, but has a complex architecture similar to that of a vascular plant. A multinucleate green alga *Caulerpa* produces complex holdfasts, stalks, and fronds up to meters in length, despite being unicellular. *Gromia sphaerica,* a testate amoeba that lives on marine sediments at depths of >1 km, produces cells up to 4 cm in diameter. There are also giant bacteria. The marine-sediment bacterium *Thiomargarita magnifica* approaches 10^{12} μm^3 in size, and *Epulopiscium,* a gut symbiont associated with surgeonfish, has a volume well over 10^{6} μm^3.

Cell size is a major organizing factor in biology, with a wide array of cellular features scaling in predictable size-dependent manners. Not all such relationships are linear, but they often unfold in ways that transcend the boundaries between major phylogenetic groups, even between prokaryotes and eukaryotes. Commonly called "laws of nature" or "rules of life," such patterns identify strict limits on what evolution has been able to achieve in the natural world. What accounts for the empty regions in phenotypic space? Are missing combinations of trait values a consequence of biophysical and/or biochemical constraints, or are certain combinations simply too disharmonious to be promoted by selection, or do both factors play a role?

The most notable of cell biology's scaling laws define the ways in which bioenergetic features relate to cell volume. These constitute the primary subject matter of the following pages, although numerous relationships for other types of traits will be explored in subsequent chapters. The focus here is on the *evolutionary* scaling of traits with size across species. There are equally compelling questions regarding

scaling relationships on nonevolutionary timescales (Marshall 2020), e.g., cellular responses to nutritional status, temperature, and other physical/chemical factors. Ultimately, we wish to know whether long-term evolutionary trajectories reflect within-species developmental responses to the environment. These issues will start to be addressed in the following chapter.

Before proceeding, a simple overview of the ways in which scaling laws are expressed and interpreted mathematically is in order. Using this framework, a number of general scaling relationships regarding energy acquisition and growth will then be summarized. This will be followed by an overview of the possible evolutionary mechanisms driving such patterns and their implications for understanding the consequences of the prokaryote-eukaryote transition.

Describing Allometric Relationships

The description of a scaling relationship between two traits demands a statistical approach, as the twin goals are generally to quantify the average pattern and degree of noise in the response of one trait to a change in the other. The relationship may be positive or negative, but provided a proportional change in one trait is associated with a constant proportional change in the other, the model can be succinctly written in the form of a simple, two-parameter power function,

$$z = \alpha S^{\beta} + e, \tag{8.1a}$$

where in this case z is the measured phenotype of interest, S is a measure of organism size (usually mass or volume), α is the fitted normalization constant (giving the expected value of z when $S = 1$), and β is the fitted scaling coefficient. Equation 8.1a indicates that, on average, a two-fold change in S is associated with a 2^{β}-fold change in z. The e term in Equation 8.1a is usually left out of such expressions (and will be from here on), but is nonetheless relevant, as it is the deviation between observed and predicted values. With appropriate statistical analysis (below), the average value of e is zero, and the magnitude of the variance of e is a measure of the goodness-of-fit of the data to the model.

There is an elegant simplicity to power functions, as they exhibit linear form when z and S are jointly transformed logarithmically. On a log scale, Equation 8.1a becomes

$$\log(z) = \log(\alpha) + \beta \log(S), \tag{8.1b}$$

providing a simple basis for estimating the parameters α and β with linear-regression analysis. The model is linear regardless of the logarithmic scale employed, e.g., base 10 as generally used here (denoted as log), or on the scale of natural logarithms (base $e \simeq 2.318$, denoted as ln). First popularized by Thompson (1917) and Huxley (1932), power-function scalings in biology are generally referred to as allometric functions, with $\beta = 1$ denoting an isometric relationship. If β is positive but < 1, then z becomes proportionally smaller with increasing S (sublinear or hypometric scaling), as $z/S = \alpha S^{\beta}/S = \alpha S^{\beta-1}$, with the exponent $\beta - 1$ being negative. In contrast, $\beta > 1$ implies supralinear or hypermetric scaling.

As will be seen below, cell biology is well-endowed with features that are reasonably described by Equation 8.1b as a first-order approximation. In principle,

although rarely relied upon, more complex functions are possible. For example, β could be a function of S. It should also be noted that the scales on which biological traits are measured are generally arbitrary, e.g., pH is measured on a log scale. Even when a particular measure does not strictly adhere to the form of Equation 8.1a, a variety of mathematical transformations to a new scale can often lead to behavior consistent with the simplest power-law form (Lynch and Walsh 1998; Frank 2016).

Regressions of trait values on organism size with slopes approximating multiples of 1/3 are particularly intriguing, as they raise the possibility of simple geometric explanations. For example, when S is on the scale of mass or volume, $\beta = 1$ suggests a mechanism directly proportional to the mass of cellular material, $\beta = 2/3$ suggests a mechanism related to surface area (because area is a function of the square and mass is a function of the cube of a length measurement), and $\beta = 1/3$ suggests a mechanism related to a linear dimension of the organism. As early investigators found numerous regression coefficients to be in the neighborhood of $x/3$ (where x is an integer value, usually 2 or 3), there was a tendency to assume they were exactly $x/3$ and then embark on proposals of mechanistic explanations for the observed patterns.

Even at an early stage in these kinds of studies, discomfort was expressed with the generality of various geometry-based hypotheses (e.g., von Bertalanffy 1957), although the tradition of searching for them continues today, with a tendency to view significant deviations as little more than annoying secondary effects. As will be discussed below, much attention has been given ideas associated with fractal delivery systems that suggest allometric coefficients of the form $x/4$ rather than $x/3$. In light of the usual uncertainties in statistical analyses, however, it is often hard to justify one of these scalings versus the other when confronted with real data. Is, for example, an estimated coefficient of $\beta = 0.29$ more consistent with $1/3 \simeq 0.33$ or $1/4 = 0.25$ scaling, or should the strict adherence to either belief be avoided?

Scaling Laws in Cellular Bioenergetics

The vast majority of work on biological scaling relationships has been performed by ecologists striving to understand the basic energetic features of ecosystems, often with a focus on multicellular taxa (e.g., Burger et al. 2019; Hatton et al. 2019). Here, our attention will be confined to the attributes of species that normally live as single cells, although as discussed in Chapter 24, there are intriguing extensions of the results for unicellular organisms to multicellular lineages. Several power-law scalings of biological features with cell size were encountered in Chapter 7 – the slightly less than linear proportionality between cell dry weight and cell volume; the decline in the fractional contribution of DNA to total cellular biomass with increasing cell size; and the sublinear scaling of the number of mRNA and protein molecules per cell with cell volume.

Strong correlational patterns imply strong constraints, and a key challenge for evolutionary cell biology is to determine their mechanistic basis. At least three classes of explanations always merit consideration: 1) inevitable outcomes of biophysical / biochemical limitations; 2) consequences of evolutionary channeling towards particular combinations of trait values that maximize fitness; and/or 3) re-

flections of drift barriers beyond which the efficiency of selection is compromised (Chapter 4).

Metabolic rate. In any discussion of size scaling of biological traits, it is appropriate to start with metabolic-rate data, as no trait has been more widely measured phylogenetically. In a statement that quickly became canonized as "Kleiber's Law," Kleiber (1932, 1947) argued that the total metabolic rate of an organism (typically measured as the rate of oxygen consumption) scales as the 3/4 power of body mass. His original analyses were largely derived from observations on vertebrates.

Although considerable subsequent research has led to a substantially altered view, West et al. (1997, 1999, 2002) have promoted the idea that quarter power-law scalings constitute universal laws relevant not just to metabolic rate but to a wide array of organismal features across the entire Tree of Life. The novelty of their work derives from a mechanistic view of fractal delivery systems (e.g., hierarchical branching networks of capillaries or leaf veins) for nutrients and respiratory gases. However, these details will not be pursued here for several reasons. First, it is unclear how the features of a branching delivery network would apply to single cells. Second, a number of questionable mathematical assumptions underlying the fractal models have been highlighted (Dodds et al. 2001; Banavar et al. 2002; Kozłowski and Konarzewski 2004, 2005; Chaui-Berlinck 2006; Apol et al. 2008), and remain despite the originators' valiant efforts to dispute them (Brown et al. 2005; Savage et al. 2007). Third, although a study with protists yielded a power-law relationship with an exponent quite close to the theoretical prediction of 3/4 (Fenchel 2014), such behavior is a simple consequence of cells evolving flatter forms as species increase their average cell volumes, and is thus explainable with a surface-area constraint model. Although discrepancies with the 3/4 rule have been made repeatedly (Dodds et al. 2001; Kozłowski and Konarzewski 2005; Glazier 2015a,b), the universality of 3/4 power-law scaling continues to be promoted (West 2017).

Not only is the allometric coefficient for metabolic rate often inconsistent with $x/4$ power-law scaling, but taken across the Tree of Life, the regression appears to be nonlinear (Zeuthen 1953). For example, with cell dry weight being the measure of size, DeLong et al. (2010) found the allometric slope for metabolic rate to be ~ 2.0 for heterotrophic bacteria and ~ 1.1 for unicellular eukaryotes. The same scaling was found whether cells were active and well-nourished or inactive and starved. Using updated cell size measurements, the allometric slopes for the two groups are more on the order of 1.3 and 1.0 (Figure 8.2). However, the two estimates are not significantly different, and although there is little overlap in cell sizes between the two groups, a hypothesis of complete continuity of scaling across both groups cannot be ruled out. Assuming an isometric relationship for eukaryotic cells, the data in Figure 8.2 imply a simple relationship, with a mean metabolic rate $\simeq 22$ nL O_2 uptake / μg cell dry weight / day (at 20° C). Using a much smaller data set based on a mixture of just eight heterotrophs and phototrophs grown at a much colder temperature (5° C), Johnson et al. (2009) again observed an isometric relationship, and suggested a universal constant equivalent to 82 nL O_2 uptake / μg cell dry weight / day. This discrepancy is not too surprising given that the range of variation around the regression in Figure 8.2 exceeds an order of magnitude.

Finally, although metabolic rate is a classical physiological measurement, read-

ily estimated as the rate of oxygen consumption or heat dissipation, its cell biological interpretation is generally far from clear. Total metabolic-rate measurements quantify the burning of carbon sources, but taken alone provide little information on the extent to which energy is converted to biomass production (growth and reproduction), the key targets of natural selection. Given the average constancy of the rate of energy utilization per unit mass noted above (independent of cell dry weight), were metabolic rate to be somehow proportional to the rate of biomass production, cell-division rates would also be expected to be nonresponsive to cell size. As discussed below, however, this expectation is far from fulfilled.

Lifetime energy requirements of a cell. Natural selection advances adaptations that enhance an organism's energetic capacity, either directly via growth and reproduction or indirectly via survivorship. However, adaptations themselves incur baseline construction and maintenance costs, and unless the benefits are sufficiently greater than the energetic costs, in the long run they will be opposed by natural selection. Furthermore, to understand the capacity of selection to incorporate adaptive modifications, we need to scale the net energetic costs and benefits relative to the total cellular energy budget (the summed costs of cell construction and maintenance per cell lifetime), as this defines the visibility of trait modifications to selection. If the relative benefits do not sufficiently outweigh the costs, the trait will be liable to loss as selection is overwhelmed by the power of random genetic drift and deleterious-mutation accumulation (Chapters 6 and 17). If the costs sufficiently outweigh the benefits, loss will be actively promoted by selection.

The total cellular energy requirements per cell cycle partition into components associated with: 1) baseline maintenance and survival; and 2) construction of the essential parts of daughter cells (for growth and reproduction). Maintenance needs include energy invested in mRNA and protein processing, osmoregulation, intracellular transport, signal transduction, motility, and DNA repair. As the length of the cell cycle is prolonged, e.g., owing to resource limitation, the total maintenance requirements per cell cycle will grow approximately linearly with the cell-division time, whereas the contribution involving the construction of new parts (a roughly one-time investment) will remain approximately constant. As a consequence, the total lifetime energetic requirements of a cell (from birth to fission) will typically increase as growth conditions decline, eventually reaching a critical point where resources are just sufficient for maintenance (with nothing left for allocation to reproduction).

A powerful empirical approach allows the partitioning of the energy associated with the maintenance and growth requirements of single-celled organisms. The method relies on estimates of the consumption rate of an energy-limiting resource at different cell-division rates (Foundations 8.1). For cells that can be grown on a defined medium in a continuous-flow chemostat (Figure 8.3), the rate of resource consumption per cell can be estimated from the difference in resource concentration between the inflow and outflow, the known cell density (which reaches an equilibrium in the growth chamber), and the flow rate. Different food resources vary in their energetic content, requiring a normalization of results across studies. However, conversion of resource consumption to units of ATP yield (the universal energy currency of cells) is readily accomplished if the metabolic pathways through which the substrate passes are known (Tempest and Neijssel 1984; Russell and Cook 1995).

The elegance of a continuous-flow culture is that an equilibrium cell-division rate is rapidly achieved, which is simply equal to the dilution rate of the chemostat. If the rate of resource consumption per cell is determined at several cell-division rates, a plot of the former vs. the latter is expected to yield a straight line, with the slope providing an estimate of the amount of resource consumed to produce a new cell, and the intercept (denoting the point at which resource consumption is insufficient to support growth) providing a measure of baseline metabolic requirements (Figure 8.3). Pioneered by Bauchop and Elsden (1960), this regression approach is often called a Pirt (1982) plot.

The general procedure has been applied to enough organisms to reveal some broad generalizations (Figure 8.4). First, the basal metabolic rate (normalized to a constant temperature of 20°C for all species) scales almost linearly with cell volume across both bacteria and eukaryotes, with an allometric relationship of

$$C_M = 0.39V^{\,0.88}, \tag{8.2a}$$

where C_M is in units of 10^9 molecules of ATP/cell/hour, and cell volume V is in units of μm^3. Care should be taken in the literal interpretation of C_M, as metabolic requirements of cells depend on their growth rates, and some maintenance activities can be strongly correlated with growth and hence reside in the estimated component for construction costs (van Bodegom 2007; Biselli et al. 2020).

Second, the scaling of the growth requirement per cell is even closer to linearity with respect to cell volume (i.e., with an exponent near 1.0),

$$C_G = 26.9V^{\,0.96}, \tag{8.2b}$$

where C_G is in units of 10^9 molecules of ATP/cell. If one further considers that a portion of eukaryotic cell volume is associated with vesicles and therefore relatively inert biologically, the regressions on active (or "effective") cell volumes might yield modified allometric scaling coefficients. Unfortunately, little information is available on the scaling of vacuolar volume with total cell size, although an analysis for photosynthetic cells suggests $\sim 89\%$ active volume for a 1-μm^3 cell, declining to $\sim 58\%$ for a 10^4-μm^3 cell (Okie 2013). Such extremes are unlikely in heterotrophic species.

The total cost of building a cell is

$$C_T \simeq C_G + t_D C_M, \tag{8.2c}$$

where t_D is the cell-division time in hours. The relationships in Equations 8.2a,b then imply that provided $t_D < 67V^{0.1}$ hours (assuming 20°C), which is generally the case in well-nourished cells, the contribution from cell growth dominates.

The preceding relationships will prove useful in subsequent chapters where attempts are made to determine the costs of various cellular features relative to a cell's entire energy budget. In Foundations 8.2, an entirely different approach to the problem, applicable to organisms that cannot be readily assayed in chemostats but for which metabolic-rate data are available, is shown to yield results that are quite compatible with Equations 8.2a,b.

Notably, both the maintenance and growth relationships scale in an apparently continuous fashion across bacteria and eukaryotes, despite the substantial difference

in cell contents between the groups. On the one hand, eukaryotic cells contain internal lipid membranes, which are energetically expensive, but on the other hand, such cells are less densely packed with biomaterials (Chapter 7).

Finally, although almost all studies on scaling relationships in biology focus on the slopes of the regressions, an equally important matter concerns the magnitude of the normalization constant. Why for example is the cost of growth of a 1-μm^3 cell $\simeq 3 \times 10^{10}$ ATP hydrolyses (Equation 8.2b), and not substantially more or less? A crude calculation suggests that this is largely a consequence of biology's reliance on ATP as an energy source and the energetic content of the biomaterials from which cells are built. From Milo and Phillips (2016), under average physiological conditions $\sim 14,300$ calories (cal) are released per mol of ATP hydrolyses, which translates into 2.4×10^{-20} cal/individual hydrolysis event. From a wide variety of sources, the energetic content of unicellular organisms is 4.7×10^{-6} cal/ng dry weight (Supplemental Table 8.1). Using these results, and converting to cell volume with the relationship in Figure 7.1, leads to an estimated cost of cell construction of $\sim 114 \times 10^9$ ATP hydrolyses/μm^3 cell volume, which is within a factor of four of the actual estimate based on elaborate work on resource consumption (Equation 8.2b).

Thus, the energetic cost of building cells is a historical legacy of the kinds of biomaterials (e.g., nucleic acids, proteins, and lipid membranes) that life has been dependent upon since the establishment of LUCA. The deeper question as to why life came to depend on ATP as a universal material for energy exchange remains unresolved.

The speed limit on cell-division rates. Natural selection feeds off of genotypic differences in rates of genome transmission on an absolute time scale. Thus, fitness ultimately depends not just on the rate of resource acquisition, but on the rate at which assimilated resources are transformed into new cells, as opposed to being burned in nonproductive activities. Thousands of studies have been performed on the growth rates of various species under a multitude of conditions, but given the diversity of approaches, the only fair comparison is to evaluate maximum known cell-division rates. Even then, the data must be normalized to a constant temperature (as the latter influences all aspects of biology; Chapter 7), and there is no guarantee that studies on any particular species have actually uncovered the optimal growth conditions.

With these caveats in mind, although the observations just discussed indicate a near constant energy cost of cells per unit volume across the Tree of Life, the rate at which biomass is constructed is far from constant. Most notably, the evolutionary relationship between maximum cell-division rate and cell size (in units of dry weight per cell) is qualitatively different between heterotrophic bacteria and eukaryotes (Figure 8.5a). Here, the growth rate is measured as the maximum exponential rate of expansion $b_{\max} = \ln(2)/t_D$, where t_D is the average cell-division time (in days). For bacteria, the scaling of this trait with cell size is positive, with an allometric coefficient of 0.28 (SE = 0.07). Although there is a more than 10$\times$ range of variation in cell-division times for any specific cell size, this is in part due to sampling error. Thus, bacteria certainly do not adhere to the idea that large cells suffer from reduced rates of cell division as a result of a surface area:volume constraint (below).

In contrast, unicellular eukaryotes universally exhibit weak, negative scaling of

maximum growth rate with cell size. For amoeboid forms, ciliates, a broad group of heterotrophic flagellates, and dinoflagellates, the allometric scaling coefficients fall in the narrow range of -0.19 to -0.22. Despite this uniform scaling over six orders of magnitude of cell-size differences, the elevation of the power-law functions vary among groups, with ciliates having the highest growth rates and flagellates the lowest.

Unfortunately, there is very little overlap in the sizes of bacterial and eukaryotic cells in these analyses of heterotrophs. Thus, it is unclear whether the observed shift in scaling behavior is a consequence of fundamental biological differences between groups or a reflection of a more general scaling relationship, with a global optimum size for cell-division rates on the order of 10^{-6} μg (fortuitously near the approximate size boundary between prokaryotes and eukaryotes). Although it may seem puzzling why all bacteria don't evolve to very large sizes and all unicellular eukaryotes to very small sizes, it should be remembered that total fitness is determined by the difference between birth and death rates, and that the optimum size for survivorship may differ greatly among environments.

Do these observations generalize to phototrophs? In general reviews of marine phytoplankton, Raven (1986, 1994) argued, with fairly limited data, that there is a reversal in the scaling of cell-division times at a cell volume of ~ 30 μm^3, which equates to an approximate cell dry weight of 10^{-5} μg, close to the area of overlap in size of bacterial and eukaryotic heterotrophs in Figure 8.5a. However, although a similar argument was made by Marañòn (2015; Marañòn et al. 2013; Ward et al. 2017), the broader comparative analysis in Figure 8.5b does not support this sort of nonmonotonic scaling for phototrophs. There is no relationship between $b_{\max}$ and cell size in cyanobacteria, and for the two eukaryotic groups with data on several dozens of species, green algae and diatoms, the allometric scaling coefficient is -0.09, which is about half that found for heterotrophs.

It bears emphasizing that the cell-division rates summarized in Figure 8.5 are all derived from pure cultures grown under optimized laboratory conditions. In nature, organisms may rarely if ever experience such conditions, commonly dividing at least one to two orders of magnitude more slowly than maximum rates. Indeed, many microbes inhabiting aquatic sediments may have generation times on the order of several years, and in some cases even hundreds to thousands of years (Hoehler and Jørgensen 2013; Morono et al. 2020). In principle, such cells may often enter semi-dormant states with maintenance requirements orders of magnitude lower than those implied in Figure 8.4 (Munder et al. 2016; Lennon et al. 2021).

To sum up, the preceding results permit three fairly general statements about the biology of cells. First, in both eukaryotes and bacteria, *absolute* rates of biomass acquisition / cell increase with cell size. This follows from the fact that the energetic requirement for growth scales nearly linearly with cell volume, i.e, as $\sim V^{0.96}$. (Figure 8.4), while cell-division times (the inverse of the division rate) scale much more weakly and even negatively with V in the case of bacteria (Figure 8.5). For both bacteria and eukaryotes, the absolute rate of production per cell increases with cell size, but it does so supralinearly with size in bacteria (because the cell-division time declines with size) but sublinearly in eukaryotic cells (because the cell-division time increases weakly with size). On the other hand, the rate of productivity per unit biomass, $b_{\max}$, which is more directly related to fitness, changes directionality

between groups, being positive in bacteria but negative in eukaryotes, yielding the pattern in Figure 8.5a.

Second, returning to the results in the previous section, insight can be gained on the efficiency of conversion of assimilated energy into growth, C_G/C_T. The lifetime cellular energy budget (C_T) is a function of the cell-division time, t_D, as $C_T = C_G + t_D C_M$ (Equation 8.2c). Using the quantitative expressions for C_G (the cost of growth) and C_M (the cost of maintenance/day) as functions of cell volume (V) in Equations 8.2a,b, and defining t_D in units of days,

$$C_G/C_T \simeq \frac{1}{1 + 0.35 t_D V^{-0.08}}. \tag{8.3}$$

Recalling from above that $t_D = \ln(2)/b_{\max}$, noting from the regression in Figure 8.5 that bacterial $b_{\max} \simeq 527 B^{0.28}$, where B is the dry weight per cell in μg, and using Equation 7.1 to express B in terms of V, leads to $t_D \simeq 0.055 V^{-0.26}$. Substitution of the latter expression into Equation 8.3 then leads to growth-efficiency estimates ranging from 0.92 to 0.99 for the range of bacterial cell volumes of 0.01 to 10 μm^3.

Thus, for bacterial cells growing at maximum rates, the vast majority of assimilated energy is allocated to growth, increasingly so in cells of larger size. With poorer growth conditions (larger t_D), these efficiencies will necessarily decline. For example, with a tenfold increase in t_D, the corresponding efficiencies become 0.79 to 0.92, and with a 100-fold increase in t_D, they reduce to 0.10 to 0.54. Thus, a lower limit to bacterial cell size arguably results from the progressive increase in the fraction of energy intake that must be devoted to maintenance in the face of a relatively long cell-division time (Kempes et al. 2012).

Growth efficiencies are somewhat lower for eukaryotic cells. For heterotrophic eukaryotic flagellates, including dinoflagellates, growing at maximum rate, $t_D \simeq 0.18 V^{0.17}$ days, efficiencies decline from 0.93 to 0.83 for cell volumes of 10 to 10^6 μm^3. For amoeboid forms, the minimum cell-division time is $t_D \simeq 0.094 V^{0.19}$ days, leading to a range for C_G/C_T of 0.95 to 0.84 for cell volumes of 100 to 10^8 μm^3. For ciliates, $t_D \simeq 0.036 V^{0.20}$ days, and C_G/C_T ranges from 0.97 to 0.92 for cell volumes of 10^3 to 10^7 μm^3. Thus, as in heterotrophic bacteria, when experiencing maximum growth capacity, most eukaryotic cells incorporate $> 90\%$ of assimilated energy into growth vs. maintenance, although the scaling of efficiency with cell volume is negative.

A final noteworthy point is that the upper halves of the dashed ellipses in Figure 8.5a demarcate apparent absolute upper-bounds to cell-division rates (normalized to 20°C) that natural selection has been able to achieve. For heterotrophic eukaryotes at this temperature, no cell divides in < 1.7 hours, and no cell > 1 μg in dry weight divides in < 8 hours. No phototroph of any size, bacterial or eukaryotic, divides in < 4 hours at 20°C. On the other hand, at the same temperature, some large bacterial heterotrophs can divide in just 15 minutes.

Can these upper limits be broken? When strong and prolonged periods of selection are imposed on growth rate in simple laboratory experiments with microbes, there can be an up to 30% increase in $b_{\max}$, e.g., in the bacterium *E. coli* (Wiser et al. 2013), the yeast *Kluyveromyces* (Groeneveld et al. 2009), and the ciliate *Tetrahymena* (Tarkington and Zufall 2021). Thus, natural selection appears to be somewhat stalled with respect to maximum growth rates, possibly because the strength of selection on maximum rates in nature is weaker than in laboratory settings where a

premium can be put on this single trait. Although it might be argued that there is a tradeoff between growth rate and competitive ability, the limited data in microbes suggests otherwise (Gounand et al. 2016).

The Limits to Natural Selection Imposed by the Drift Barrier

The classical dogma in physiological ecology is that scalings of bioenergetic features are unavoidable constraints of biochemistry and/or biophysics. As outlined in detail by West (2017), numerous arguments based on organism size lead to power-law behavior with exponents being multiples of 1/3 or 1/4 depending on one's mechanistic perspective. However, although such hypotheses are based on what may appear to be reasonable arguments, the inferred supportive evidence almost always derives from statistical analysis of patterns rather than on direct experimental evidence of mechanistic constraints. Moreover, as noted above, a more fundamental problem is that neither 1/3 nor 1/4 power-law scalings provide general explanations for the phylogenetic patterning of bioenergetic traits in unicellular organisms.

Most striking are the opposite directions of scaling of maximum growth rate and efficiency with cell size in bacteria vs. eukaryotes. For bacterial growth rates, the scaling is positive, although the data are noisy enough that the true exponent could be anywhere in the range of 0.14 to 0.42. In contrast, the scaling exponents for individual heterotrophic unicellular eukaryotic groups are not only negative, but more compatible with $-1/5$ than either $-1/4$ or $-1/3$ power-law scaling. For phototrophs, the growth-rate scaling exponent is even weaker than $-1/5$, being closer to $-1/10$.

This lack of robust support for biophysical-constraint hypotheses suggests a need to evaluate the problem of growth-rate scaling from an entirely different perspective. Shifting the view from biophysical constraints to limits on the evolutionary process, one possibility is that with increasing cell size, the efficiency of natural selection declines, owing to the associated reduction in effective population size (N_e). The intention here is not to promote the idea of precise 1/5 (or 1/10) power-law scaling relationships. Further empirical study of the distribution of mutations with small effects in various phylogenetic lineages will be necessary for that level of resolution. The key point is that any reduction in N_e will diminish the ability of natural selection to purge deleterious mutations, thereby leading to a reduction in trait performance.

If this hypothesis is correct, arguments that attempt to explain scaling patterns across the Tree of Life purely on the basis of cell-geometric arguments will be incomplete, if not entirely misplaced. If, on the other hand, it could be shown that the population-genetic environment has no influence on scaling relationships, this would imply that the structure of cell biology is such that there is always a supply of mutations with sufficiently large, variable, and beneficial effects to bring things to their biophysical limits regardless of phylogenetic affinity.

Recall from Chapter 4 that the key determinant of whether natural selection can eradicate a deleterious mutation with effect s is whether the ratio of the power of selection to the power of drift $s/(1/N_e) = N_e s$ exceeds 1.0. The fact that N_e scales with the -0.20 power of organism size (Figure 4.3) implies that species with larger cell sizes have reduced capacities to promote growth-rate promoting mutations and to

eradicate growth-rate reducing mutations of small effects. As noted in Chapter 5 and further elaborated on in Chapter 17, the evidence is compelling that a large fraction of mutations have fitness effects (s) below $|s| = 10^{-5}$, extending down to 10^{-10} or even lower in species with larger cell sizes. Because N_e in unicellular species is typically in the range of 10^6 to 10^9 individuals, this means that a substantial number of mutations with individually very mildly deleterious (i.e., growth-reducing) effects are free to accumulate in species with relatively small N_e while still being subject to efficient purging in larger-N_e species.

As discussed in Chapter 4, several genetic features determine how the efficiency of selection against mildly deleterious mutations scales with the demographic features of a population. These are evaluated in a stepwise fashion in the next few paragraphs to show how the progressive incorporation of natural genomic features can plausibly lead to the kinds of negative scaling seen in Figure 8.5.

The simplest starting point assumes that selection operates on individual genetic loci independently of events occurring at other genomic locations. This requires either very high recombination rates or such small population sizes that cosegregating variants are never simultaneously present at multiple loci. Consider the situation in which each locus harbors two possible alleles, + (beneficial) and − (deleterious), with the mutation rates from + to −, and vice versa, being u_{10} and u_{01}, and the + allele having advantage s. At small enough population sizes that $N_e s \ll 1$, the long-term average frequency of the favorable + allele is simply a function of the ratio of mutation rates, $u_{01}/(u_{01} + u_{10})$, but as the condition $N_e s \gg 1$ is approached, the increased efficiency of selection drives the mean frequency to 1.0 (Figure 8.6a). Under this model, the transition between these two extremes occurs in a narrow (order of magnitude) range of N_e. Thus, this simple model is inadequate to explain a consistent scaling of mean performance across several orders of magnitude of population size.

Suppose, however, that there are multiple, completely linked loci with the same mutational and selection properties, with a haplotype's growth rate being determined in an additive fashion (proportional to the fraction of loci occupied by + alleles), and fitness being defined by a multiplicative (independent effects) model, $(1-s)^n \simeq e^{-sn}$, where n is the number of − alleles. In this case, it can take as many as five orders of magnitude of N_e to span the full range of equilibrium mean growth rate (Figure 8.6b). This shift in behavior is a consequence of selective interference among simultaneously segregating mutations, as described in Chapter 4. For populations of moderate size, there will be genetic variation among individuals in terms of the total number of + alleles harbored across loci, the result being that many new beneficial mutations will arise on suboptimal genetic backgrounds destined to eventual loss. At the largest population sizes, however, selection still keeps deleterious alleles at very low frequencies at all genomic sites, reducing the effects of background interference.

A third issue to consider is that fitness effects will vary among genomic sites, with sites with large effects likely being much rarer than sites with small effects (Chapter 5). This further flattens the scaling of mean trait performance with organism / population size. Even with free recombination, such behavior results because the sites with progressively smaller effects require increasingly high N_e for selection to promote their favorable alleles. As a consequence, the equilibrium mean perfor-

mance will be a mixture of the responses found for the fixed-effects model. This can be observed as the stepwise increment in mean performance in Figure 8.6c where there are sites with just three different effects, but a smoother transition would arise with a more continuous distribution of site effects.

Finally, Figure 8.6d considers the situation in which different types of sites are completely linked. In this case, as a site with major effects becomes surrounded by increasing numbers of minor-effect sites, there is again a progressive decline in the rate of scaling of mean performance with N_e. Increasing numbers of minor-effect loci cause increased background interference for selection operating on major-effect sites, while also contributing more to the total maximum performance of the trait (diluting the overall influence of the major-effect sites).

Without a detailed understanding of the fine-scaled distribution of genomic sites with different magnitudes of mutational effects, a precise statement cannot be made on the expected scaling relationship between mean performance and N_e, other than that it should be negative. This might be viewed as a short-coming of the theory. However, it should be recalled that virtually all biophysical explanations simply adhere to the assumption of a fixed power-law relationship, even when the latter can be shown to be not generalizable. The main limitation of the drift-barrier hypothesis is not an absence of generalizable theory, but a lack of precise information on mutations with small effects.

For a trait like growth rate, it can be expected that essentially every genomic site influences performance in at least a small way, and that there will be considerable variation among nucleotide sites in terms of average effects and recombination rates. Thus, because the plotted theoretical results encompass a wide range of plausible genetic properties, it is clear that there is little justification for ignoring the possibility that the variation in the population-genetic environment plays a significant role in defining relationships between maximum performance, organism size, and N_e. For this not to be the case, all deleterious mutations would have to have effects smaller than the smallest $1/N_e$ (from Figure 4.3, on the order of 10^{-9}), and hence to be impervious to selective removal in all organisms, and/or larger than the largest $1/N_e$ (on the order of 10^{-4}), and hence impervious to fixation across the Tree of Life. It is highly implausible that no mutations would have fitness effects in the range of 10^{-9} to 10^{-4}.

What can be said is the following. For heterotrophic eukaryotes, both $b_{\max}$ and N_e scale with the -0.2 power of body mass, which means that species-specific $b_{\max}$ is directly proportional to N_e. Thus, for every fractional decline in N_e, there is an equal fractional decline in $b_{\max}$, and this is consistent over the entire span of N_e. For this to occur, within the window of mutations with selection coefficients in the range of 10^{-9} to 10^{-4}, there must be an inverse relationship between the number and effects of mutations, such that the product remains constant over this full range of s.

To see this, note that for the interval of N_e between 10^4 and 10^5, there will be an interval of deleterious mutations with s in the range of 10^{-5} to 10^{-4} that are vulnerable to fixation by drift, but would be efficiently purged by natural selection for $N_e > 10^5$. Likewise, for the interval of N_e between 10^5 and 10^6, there will be an interval of deleterious mutations with s in the range of 10^{-6} to 10^{-5} that are vulnerable to fixation by drift, but would be efficiently purged by natural selection

at $N_e > 10^6$, and so on. Thus, for the interval-specific decline in $b_{\max}$ to remain constant across N_e, the number of relevant mutational effects in each interval must be inversely proportional to the effects, such that the product remains constant. Such a negative exponential distribution of fitness effects is at least qualitatively compatible with what we know about the subject within various species (Chapters 5 and 17). It should be noted, however, that the concern here is with the cross-phylogeny balance of load-creating mutations, with the total load of mutations with effect $s \simeq 1/N_e$ remaining approximately constant as N_e changes across lineages.

Owing to insufficient information on N_e in phototrophs, this type of argument cannot be quantitatively extended to this group, although the exact argument would apply if N_e happened to scale with the -0.1 power of body mass in phototrophs. There is a similar lack of information on the scaling of N_e with cell size in prokaryotes. However, given that $b_{\max}$ increases with cell size in bacteria, and assuming that N_e scales negatively with cell size (as in eukaryotes), the drift-barrier hypothesis cannot explain the size-specific growth scaling in bacteria. The possibility is then raised that adaptive evolution in bacteria is typically nearly invulnerable to compromises resulting from drift. Assuming an upper limit to $N_e \simeq 10^9$, this would require that the vast majority of deleterious mutations in such species have $s > 10^{-9}$, as suggested in Chapter 5.

Membrane Bioenergetics and the Prokaryote-Eukaryote Transition

As noted in Chapter 2, a peculiar feature of cell biology is the localization of the key machinery associated with energy production to lipid bilayers. The series of complexes known as the electron transport chain (ETC) couple the extraction of electrons from the oxidation of organic compounds to the export of hydrogen ions, maintaining a concentration gradient of the latter across the membrane. The biochemical details of this process are covered in all biochemistry texts, and will not be elaborated upon here. The salient issue is that the cross-membrane gradient in hydrogen-ion concentration driven by the ETC causes chemiosmotic pressure for the return movement of hydrogen ions through membrane-embedded ATP synthase complexes, which couple this mechanical energy to the production of ATP (Chapter 2). One of the key differences between prokaryotes and eukaryotes is that in the former all of these events take place on the inner cell membrane, whereas membrane bioenergetics has been relocated/restricted to the inner membranes of mitochondria in eukaryotes (where they would have been present from the outset in the primordial mitochondrion; Chapter 23).

Under the assumption that energy production is limited by the number of ATP synthase complexes, which in turn are assumed to be limited by the availability of plasma membrane-surface area, Lane (2002, 2015, 2020; Lane and Martin 2010) argued that the endosymbiotic establishment of mitochondria freed eukaryotes of this constraint by providing effectively unlimited inner mitochondrial membranes. This assertion led to the further claim that the energetic boost made possible by mitochondria constituted a watershed moment in evolution by generating excess power essential to all things associated with eukaryogenesis. Under this view, the mitochondrion is not simply one of the many unique features of eukaryotes. Rather,

it is the key feature that enabled the evolution of internal cell structure, large cell size, expanded genomes, multicellularity, sex, behavior, etc., all of which are viewed as hallmarks of organismal superiority.

Before evaluating the likelihood of this scenario, a brief consideration of the surface-area problem is in order. The general formulae for several common cell shapes are provided in Table 8.1. Regardless of the shape, volume always increases with the cube of a linear dimension, whereas the surface area increases with the square of the linear measure. The surface-area to volume ratio depends on shape, but it is always inversely related to a linear dimension of the cell.

Because the production of ATP in prokaryotes is highly dependent on complexes embedded in the plasma membrane, the geometric-constraint argument implies that if the cell surface is a limiting resource, there should be a reduction in energy production per unit volume with increasing cell size. However, the analyses in the previous section already shed doubt on this assertion, showing that increased cell size is associated with higher, not lower, maximum rates of growth in bacterial species. In contrast, mitochondria-bearing eukaryotes have lower energetic capacities than prokaryotes on a volumetric basis, and growth rates decline with with increasing cell size. This matters from an evolutionary perspective because it is the growth rate per unit volume, often called the specific growth rate, that determines the rate of gene flow into the next generation. Thus, observations on the growth-rate potential across the Tree of Life are uniformly inconsistent with the basic premise underlying the Lane hypothesis.

Table 8.1. Geometric features for cells of common shapes. Abbreviations: $r < \ell$, radii or half-widths for spheroids; h, full length of a cylinder or rod; $\alpha = h/r$ or ℓ/r. Note that for a rod, h is the length from one rounded tip to the other. The formula for the surface area of a spheroid is known as Knud Thomsen's approximation.

Shape	Surface Area (S)	Volume (V)	S/V
Sphere	$4\pi r^2$	$(4/3)\pi r^3$	$3/r$
Cylinder	$2\pi r(r+h)$	$\pi r^2 h$	$2(1+\alpha)/h$
Rod	$2\pi rh$	$\pi r^2[h-(2r/3)]$	$(2\alpha/r)/[\alpha-(2/3)]$
Prolate spheroid	$2.02\,\pi r^2(1+2\alpha^{1.61})^{0.63}$	$(4/3)\pi r^2\ell$	$(1.5/\ell)(1+2\alpha^{1.61})^{0.63}$

Energy production and the mitochondrion. A consideration of eukaryotic cell anatomy provides a more mechanistic view of why the total membrane energetic capacity of eukaryotic cells is nothing out of the ordinary. A key question is whether mitochondria endow eukaryotic cells with enhanced membrane surface area for the occupancy of ATP synthase. Although the situation at the time of first colonization of the mitochondrion is unknown, the iconic view of mitochondria being tiny, bean-shaped cellular inclusions is not generalizable. For example, many unicellular eukaryotes harbor just a single mitochondrion or one that developmentally moves among alternative reticulate states (e.g., Burton and Moore 1974; Rosen et al. 1974; Osafune et al. 1975; Biswas et al. 2003; Yamaguchi et al. 2011; Uwizeye

et al. 2021). Such geometries necessarily have lower total surface areas than a collection of spheroids with similar total volumes. For the range of species that have been examined, many of which do have small individualized mitochondria, the total outer surface area of mitochondria per cell is generally on the order of the total area of the plasma membrane, with no observed ratio exceeding 5:1, and ratios for the smallest species being less than 1:5 (Figure 8.7a). Given the putative archaeal nature of the cell that hosted the primordial mitochondrion (Chapters 3 and 23), it is likely that the starting condition resembled the situation in today's smallest eukaryotes.

Although the outer surface area of the mitochondrion has been the most common source of measurements, it is less relevant than the inner membrane, where the ATP synthase complex sits. However, for the few species with available data, the ratios of inner to outer membrane areas for mitochondria are modest – ∼5.0, 2.4, 2.5, and 5.2, respectively, in mammals, the green alga *Ochromonas,* the plant *Rhus toxicodendron,* and the ciliate *Tetrahymena* (summarized in Lynch and Marinov 2017). Moreover, the total surface areas of mitochondria substantially overestimate the real estate allocated to ATP synthase complexes, which are often restricted to two rows on the narrow edges of the inner invaginations (called cristae), often comprising $\ll 10\%$ of the total internal membrane area (Kühlbrandt 2015).

Three additional observations raise further questions as to whether membrane surface area is a limiting factor in ATP synthesis. First, multiple observations on the developmental responses of organelles to cell growth indicate that the total mitochondrial volume remains proportional to cell volume (Atkinson et al. 1974; Grimes et al. 1974; Posakony et al. 1977; Pelligrini 1980; Rafelski et al. 2012), and the same has been observed in the comparative analysis of protist species (Fenchel 2014). From arguments in the preceding section, this implies that the surface area of mitochondria scales with the 2/3rds power of cell volume. Thus, if mitochondrial surface area limits cellular energy production, to maintain mitochondrial generating power capacity per unit volume, the concentration of mitochondria would need to scale as $V^{1/3}$ rather than following the observed volume-independent pattern. Second, only a fraction of bacterial membranes appears to be allocated to bioenergetic functions (Magalon et al. 2015), again shedding doubt on whether membrane area is a limiting factor for prokaryotic energy production. Third, as will be discussed more fully in Chapter 9, in every bacterial species for which data are available, growth in cell volume is exponential or close to it. Thus, as in the among-species pattern (Figure 8.5), growth rates of individual bacterial cells increase with cell volume despite the reduction in the surface area:volume ratio.

Still further insight into this issue derives from the average packing density of ATP synthase for the few species with sufficient proteomic data (Lynch and Marinov 2017). For example, the estimated number of complexes in *E. coli* is ~ 3000, and the surface area of the cell is $\sim 16\ \mu m^2$. A single ATP synthase in this species occupies $\sim 64\ nm^2$ (Lücken et al. 1990) of surface area, so the total set of complexes occupies $\sim 2\%$ of the cell membrane. Drawing from additional observations on four other diverse bacterial species, the overall average membrane occupancy of ATP synthase is just 1% in bacteria (Lynch and Marinov 2017).

This kind of analysis can be extended to the few eukaryotes for which data are available, noting that eukaryotic ATP synthases are slightly larger, with maximum

surface area of ~ 110 nm^2 (Abrahams et al. 1994; Stock et al. 1999). Although ATP synthase resides in mitochondria in eukaryotes, it is relevant to evaluate the fractional area that would be occupied were they to be located in the cell membrane. Such hypothetical packing densities are 5 to 7% for yeast and mammalian cells (Lynch and Marinov 2017). (Adding in the membrane occupancy of the entire ETC would increase these proportions by ~ 4-fold, in both prokaryotes and eukaryotes). These observations suggest a ~ 5-fold increase in ATP synthase abundance relative to cell-surface area expectations in eukaryotes, although the data conform to a continuous allometric function with no dichotomous break between bacteria and eukaryotes (Figure 8.7b).

To sum up, these multifaceted observations are consistently contrary to the idea that the relocation of membrane bioenergetics endowed eukaryotes with enhanced growth efficiency beyond what would be expected of bacterial cells of similar size. Indeed, if there are any effects at all, they appear to be negative. One could perhaps argue that eukaryotes would be even poorer growers were it not for the presence of mitochondria, but extrapolations into the realm of unobserved data is inadvisable, the ancient belief in a flat Earth being a well-known example.

Cellular investment in ribosomes. The ribosome content of a cell provides another strong indicator of its bioenergetic potential, translation capacity in particular. Owing to the large number of proteins required to build the complex, ribosomes are energetically costly, and the number per cell within a species appears to be universally correlated with cellular growth rate. At low nutritional states, cells reduce their investments in ribosomes relative to components of the cell involved in nutrient uptake (Chapter 9). One might then expect variation in the translational capacity of cells of different species to reflect their intrinsic bioenergetic potential.

As noted in Chapter 7, the genome-wide total and mean number of transcripts per gene scale with cell volume as $V^{0.42}$ and $V^{0.26}$ respectively, and the analogous scalings for proteins are $V^{0.95}$ and $V^{0.65}$, with no dichotomous break between prokaryotes and eukaryotes (Lynch and Marinov 2015). As with the transcripts they process and the proteins they produce, the numbers of ribosomes per cell also appear to scale sublinearly with cell volume, $\propto V^{0.80}$, in a continuous fashion across bacteria and unicellular eukaryotes, including cultured cells from multicellular species (Figure 8.8). Note that under the assumption that ribosomes produce proteins at approximately constant rates in different organisms, the scaling of protein production per volume would be $V^{0.80}/V = V^{-0.20}$. Thus, the cellular concentration of ribosomes matches the scaling of maximum growth rates with eukaryotic cell size outlined in Figure 8.5.

The mitochondrion as a driver of eukaryotic evolution. Lane (2015) and Lane and Martin (2010) have proposed a scenario for how the mitochondrion became established by a series of adaptive steps, arguing that the eukaryotic leap to increased gene number and cellular complexity, and a subsequent adaptive cascade of morphological diversification "was strictly dependent on mitochondrial power." A similar argument was made by DeLong et al. (2010), and many others have repeated the narrative that eukaryogenesis and all of the associated downstream effects would

be impossible without mitochondria.

However, as should now be clear, there is no evidence in support of this hypothesis. Indeed, diverse sets of comparative observations all lead to the opposite conclusion. Large bacterial cells do not suffer from reduced rates of biomass production, but eukaryotic cells do. There is not a quantum leap in the surface area of bioenergetic membranes in eukaryotes. The idea that ATP synthesis is limited by total membrane surface area is not supported. Moreover, the numbers of ribosomes and ATP synthase complexes per cell, joint indicators of a cell's capacity to convert energy into biomass, scale with cell size in a continuous fashion both within and between bacterial and eukaryotic groups. In addition, as will be noted in subsequent chapters, the absolute costs of producing not only ribosomes but the remaining proteins in cells (the members of the electron-transport chain in particular) are significantly higher in eukaryotes than in bacteria, owing to the substantial increase in complex size, gene lengths, investment in nucleosomes, etc. Finally, there is the additional matter of the expense of building mitochondria, associated with the high biosynthetic costs of lipid bilayers (Chapter 15).

More will be discussed with respect to the origin of the mitochondrion in Chapter 23, but the idea that the mitochondrion engendered a bioenergetics revolution can be put to rest for now. The relocation of membrane bioenergetics to inner mitochondrial membranes may have endowed eukaryotes with novel possibilities for further remodeling of cellular features. But an enhanced capacity for transforming energy into biomass was not one of them.

Summary

- Cell volumes vary by approximately eleven orders of magnitude across the Tree of Life, with most being in the range of 10^{-3} to 10^{8} μm^3 in volume. Although most prokaryotic cells are < 10 μm^3 in size, a few giants exceed 10^{9} μm^3, and a few unicellular eukaryotes with complex morphology are orders of magnitude larger.

- Species-specific mean phenotypes for various traits often scale in a continuous manner with cell size, implying substantial constraints on evolutionary diversification. A central goal of evolutionary cell biology is to determine the degree to which such patterns are consequences of biophysical constraints, selective disadvantages of discordant combinations, and/or outcomes of a reduction in the efficiency of selection that increases with cell size.

- One of the most studied physiological traits is metabolic rate, which scales positively with cell volume in a nearly isometric fashion in unicellular species. Such behavior is inconsistent with the 2/3 or 3/4 power-law scaling often invoked in the literature for multicellular species. Despite their ease of acquisition, metabolic-rate measures provide little insight into the basic currency of natural selection. However, when combined with growth-rate data, they can yield information on

the efficiency of the rate of conversion of food resources into growth and reproduction.

- The energetic costs of constructing and maintaining cells scale nearly isometrically with cell volume across the Tree of Life, despite the significant differences in cellular architectures between prokaryotes and eukaryotes. The ultimate biophysical/evolutionary constraints on the total costs per unit volume remain to be determined, but it is relevant that the caloric content of biomass exhibits little phylogenetic variation.

- Maximum cell-division rates scale positively with cell size among heterotrophic bacterial species, but negatively among eukaryotic heterotrophs. Similarly, there is a directional shift in the efficiency of conversion of energy to growth in heterotrophic bacteria vs. unicellular eukaryotes, with growth efficiency being lowest in large eukaryotic cells, and highest in large prokaryotic cells.

- The precise mechanisms that define the upper limits to growth rate remain unresolved, but the case can be made that the negative scaling with cell size in eukaryotes is at least in part a consequence of the reduced efficiency of natural selection operating on growth-rate related mutations in organisms with progressively larger cell size. As cell size increases, the effective population size decreases, and a larger number of mild growth-rate reducing mutations are free to drift to fixation.

- It is commonly asserted that the establishment of the mitochondrion released the host eukaryotic cell from a surface area:volume constraint, precipitating a bioenergetic revolution. However, a diversity of observations, ranging from the scaling of energetic traits with cell size to the anatomy and cellular content of mitochondria, ATP synthase, and ribosomes, are inconsistent with this hypothesis.

Foundations 8.1. The cost of building a cell. Cell-division rates ultimately depend on the rate of acquisition of energy necessary to build a new cell. Arguably, the best currency to use in such analyses is units of ATP usage, as it is the hydrolysis of phosphate bonds in the conversion of ATP to ADP (and in some cases, ADP to AMP, or GTP to GDP) that delivers the vast majority of energy for cellular functions. In principle, with a solid enough understanding of biosynthetic pathways and the various inputs of cellular resources, one could calculate the total energy required to build a cell by summing over the demands for the replacement of proteins, nucleic acids, lipids, etc. However, energy transformation is not 100% efficient, cellular components turn over on time scales less than the life of a cell, and energy must be invested into additional maintenance functions. Thus, the total energy utilized by a cell before giving rise to two daughters must exceed the cost of producing the standing levels of cellular components. This total level of investment (maintenance plus construction) represents the net cost of building a cell.

Determining the quantities of interest here is generally difficult for cells growing in natural environments, as most heterotrophic organisms consume a variety of resources varying in energy content. Thus, most knowledge in this area is derived from the growth of microorganisms on a defined medium, with a single limiting carbon/energy source that enters a metabolic pathway with well-understood ATP-generating properties. If the organism can be grown in a chemostat (Figure 8.3a), it is straight-forward to calculate both the rate of cell division and the rate of substrate consumption, and therefore to obtain the ratio, i.e., the yield of cells per unit consumption.

Data derived from such analyses were the source of the information presented in the preceding chapter on yields of biomass per unit carbon consumption (Figure 7.8). However, as previously noted, the level of yield depends on the nature of the carbon source, so a more meaningful measure focuses on a secondary conversion to the yield per unit ATP hydrolysis. Such a measure is more generalizable, as it accounts for differences in energetic contents among alternative carbon sources.

A chemostat (Figure 8.3a) consists of a closed environment in which sterilized medium is pumped in at a defined rate, with resource-depleted effluent (including the cells suspended within it) being eliminated at the same rate. If such a system is seeded with a pure population of a microbe, after several rounds of cell division, the population size will reach a steady state defined by the flow rate and the nutrient concentration. At this point, the population will have grown to a density at which the cell-division rate b equals the dilution rate d (i.e., the flow rate divided by the culture volume). The rate of resource consumption per cell is then equal to the rate of loss of substrate (the flow rate times the concentration difference between the inflow and outflow) divided by the number of cells in the steady-state culture.

Joint insight into maintenance and growth requirements is acquired by culturing cells under different flow rates. Such treatment imposes different nutritional states, as low and high dilution rates lead to high and low population densities (and hence low and high nutrient availabilities per cell). Assuming a constant rate of resource consumption per cell necessary for maintenance (C_M), the consumption rate (per unit time) at cell-division rate b (equivalent to the dilution rate d) can be written as

$$C = C_M + (b \cdot C_G) \tag{8.1.1}$$

where C_G measures the total growth-related consumption per cell division (Tempest and Neijssel 1984; Russell and Cook 1995). From a fitted least-squares regression of observed consumption rates C against growth rates b, the intercept and slope respectively estimate the cellular requirements for maintenance per unit time and growth per cell division, C_M and C_G (Figure 8.3b).

The total cost of producing a cell at any growth rate b can be obtained by multiplying the consumption rate C by the mean cell-division time, which is equivalent to the reciprocal of the cell division rate, $1/b$,

$$C_T = (C_M/b) + C_G, \tag{8.1.2}$$

Provided the assumption of a constant rate of basal metabolism independent of the growth rate is correct, this means that lifetime resource requirements are higher in slower-growing cells owing to the increased cumulative maintenance requirements under a longer lifespan. (The first term in Equation 8.1.2 scales with the cell-division time).

In the preceding formula, the units associated with C_T and C_G are of the form (amount of resources consumed)/cell. Here, however, we are interested in defining C_T to be the number of ATP hydrolyses required to yield a new cell, so appropriate conversions need to be made. C_G is then defined as the total number of ATP hydrolysis equivalents consumed in the production of building blocks leading to an offspring cell (independent of time), and C_M as the number of ATPs utilized per cell per unit time for maintenance. The quantity $1/C_G$ is often denoted as $Y_{\max}$, as it represents the yield of cells per unit resource consumption that would occur in the absence of basal cellular requirements.

Although the general approach just taken assumes that metabolic requirements are constant, independent of the rate of growth, alternative formulations have been developed for the situation in which there is an additional metabolic cost to growth (Tempest and Neijssel 1984; Wieser 1994; Russell and Cook 1995). Note, however, that if maintenance costs are linearly related to the growth rate, this additional contribution is simply contained within the term C_G in Equation 8.1.1, but in principle, a term that is a nonlinear function (e.g., a quadratic) of b can be included. Although such alternative expressions can yield somewhat different interpretations on how energy is partitioned as a function of the growth environment, the total energy requirement observed at any particular growth rate remains unambiguous.

Foundations 8.2. Connecting metabolic rates with growth potential. The power of the preceding (Pirt-plot) approach is that it can be applied to any sort of energy source, provided proper conversion to the level of ATP equivalence can be made. However, aside from the laborious nature of maintaining chemostats, the challenges become almost insurmountable with organisms requiring a complex diet, as is the case for the heterotrophic eukaryotes that make a living by consuming other cells. The problem here is that food resources consisting of undefined molecular mixtures cannot be converted to ATP equivalents based on basic biochemical principles.

For this reason, we turn to a second approach, motivated by the potential utility of joint information on metabolic rate and growth rate in unicellular species. If one has joint information on the rate of oxygen consumption (M, numbers of O_2 molecules consumed/cell/time) and the rate of cell division (R, the inverse of the cell doubling time), M/R provides an estimate of the number of O_2 molecules consumed per cell division. (Because metabolic rates are generally recorded as volumetric consumption rates, to obtain M, the appropriate conversion of units needs to be made. For example, at standard biological temperatures and pressures, 1 L (liter) $O_2 \simeq 0.045$ mol O_2, and multiplying by Avogadro's number yields 2.7×10^{22} molecules of O_2/liter). Basic observations from biochemistry (Foundations 17.2) indicate that the number of ATPs produced per oxygen atom consumed (the so-called P:O ratio; Mookerjee et al. 2017) $\simeq 2.5$, so under steady-state assumptions, $5M/R$ provides an estimate of the number of ATP hydrolyses per cell division (as the number of ATPs per O_2 is 5).

A final key issue here is that $5M/R$ only represents the fraction of carbon resources allocated to energy production (θ), the remainder being used as carbon skeletons in biomass production. Analysis of the biosynthetic pathways of amino acids, nucleotides, and lipids leads to estimates of $\theta = 0.21$, 0.17, and 0.27, respectively (Chapter 17). As there are numerous, small additional ATP-consuming costs associated with biomass assembly, e.g., polymerization, protein folding, cargo delivery, mRNA replacement, etc. (Lynch and Marinov 2015, 2017), and nucleotides comprise a minor fraction of total biomass, a reasonable first-order approximation for cell-wide θ is then 0.5, and dividing $5M/R$ by this leads to

$$C'_G \simeq \frac{10M}{R}, \tag{8.2.1}$$

as an alternative measure of the total energetic requirements for daughter-cell construction (again, in units of ATP-hydrolysis equivalents). The utility of this approach is the lack of requirement for detailed knowledge of the nature of the food supply, which instead is reflected in the more easily observed metabolic rate.

As an explicit example of the utility of this approach, we consider a broad set of data for ciliate species with nearly a nearly 10,000-fold range of variation in cell size (Figure 8.9). The rate of cell division (per day) scales negatively with cell dry weight (B, in ng),

$$R \simeq 5.6B^{-0.22}, \tag{8.2.2a}$$

whereas the metabolic rate (molecules O_2/cell/day) scales positively

$$M \simeq (3.4 \times 10^{13})B^{0.62}, \tag{8.2.2b}$$

yielding

$$C'_G \simeq (6.1 \times 10^{13})B^{0.84}. \tag{8.2.2c}$$

This can be compared to the regression based on Pirt-plot analyses (Equation 8.2b), which after conversion of cell volume to cell dry weight becomes

$$C_G \simeq (6.7 \times 10^{13})B^{1.05}. \tag{8.2.3}$$

Thus, the two approaches give fairly similar results, although the Pirt-plot formula (to which only a single ciliate contributes) is closer to an isometric relationship.

Literature Cited

Abrahams, J. P., A. G. Leslie, R. Lutter, and J. E. Walker. 1994. Structure at 2.8 A resolution of F1-ATPase from bovine heart mitochondria. Nature 370: 621-628.

Apol, M. E. F., R. S. Etienne, and H. Olff. 2008. Revisiting the evolutionary origin of allometric metabolic scaling in biology. Func. Ecol. 22: 1070-1080.

Atkinson, A. W. Jr., P. C. John, and B. E. Gunning. 1974. The growth and division of the single mitochondrion and other organelles during the cell cycle of *Chlorella,* studied by quantitative stereology and three dimensional reconstruction. Protoplasma 81: 77-109.

Banavar, J. R., J. Damuth, A. Maritan, and A. Rinaldo. 2002. Supply-demand balance and metabolic scaling. Proc. Natl. Acad. Sci. USA 99: 10506-10509.

Bauchop, T., and S. R. Elsden. 1960. The growth of micro-organisms in relation to their energy supply. J. Gen. Microbiol. 23: 457-469.

Biselli, E., S. J. Schink, and U. Gerland. 2020. Slower growth of *Escherichia coli* leads to longer survival in carbon starvation due to a decrease in the maintenance rate. Mol. Syst. Biol. 16: e9478.

Biswas, S. K., M. Yamaguchi, N. Naoe, T. Takashima, and K. Takeo. 2003. Quantitative three-dimensional structural analysis of *Exophiala dermatitidis* yeast cells by freeze-substitution and serial ultrathin sectioning. J. Electron Microsc. (Tokyo) 52: 133-143.

Brown, J. H., G. B. West, and B. J. Enquist. 2005. Yes, West, Brown and Enquist's model of allometric scaling is both mathematically correct and biologically relevant. Func. Ecol. 19: 735-738.

Burger, J. R., C. Hou, and J. H. Brown. 2019. Toward a metabolic theory of life history. Proc. Natl. Acad. Sci. USA 116: 26653-26661.

Burton, M. D., and J. Moore. 1974. The mitochondrion of the flagellate, *Polytomella agilis.* J. Ultrastruct. Res. 48: 414-419.

Chaui-Berlinck, J. G. 2006. A critical understanding of the fractal model of metabolic scaling. J. Exp. Biol. 209: 3045-3054.

DeLong, J. P., J. G. Okie, M. E. Moses, R. M. Sibly, and J. H. Brown. 2010. Shifts in metabolic scaling, production, and efficiency across major evolutionary transitions of life. Proc. Natl. Acad. Sci. USA 107: 12941-12945.

Dias-Lopes, G., J. R. Wiśniewski, N. P. de Souza, V. E. Vidal, G. Padrón, C. Britto, P. Cuervo, and J. B. De Jesus. 2018. In-depth quantitative proteomic analysis of trophozoites and pseudocysts of *Trichomonas vaginalis.* J. Proteome Res. 17: 3704-3718.

Dodds, P. S., D. H. Rothman, and J. S. Weitz. 2001. Re-examination of the "3/4-law" of metabolism. J. Theor. Biol. 209: 9-27.

Fenchel, T. 2014. Respiration in heterotrophic unicellular eukaryotic organisms. Protist 165: 485-492.

Frank, S. A. 2016. The invariances of power law size distributions. F1000 Res. 5: 2074.

Glazier, D. S. 2015a. Body-mass scaling of metabolic rate: what are the relative roles of cellular versus systemic effects? Biology (Basel) 4: 187-199.

Glazier, D. S. 2015b. Is metabolic rate a universal 'pacemaker' for biological processes? Biol. Rev. Camb. Philos. Soc. 90: 377-407.

Grimes, G. W., H. R. Mahler, and R. S. Perlman. 1974. Nuclear gene dosage effects on mitochondrial mass and DNA. J. Cell Biol. 61: 565-574.

Groeneveld, P., A. H. Stouthamer, and H. V. Westerhoff. 2009. Super life – how and why 'cell selection' leads to the fastest-growing eukaryote. FEBS J. 276: 254-270.

Hatton, I. A., A. P. Dobson, D. Storch, E. D. Galbraith, and M. Loreau. 2019. Linking scaling laws across eukaryotes. Proc. Natl. Acad. Sci. USA 116: 21616-21622.

Hoehler, T. M., and B. B. Jørgensen. 2013. Microbial life under extreme energy limitation. Nat. Rev. Microbiol. 11: 83-94.

Huxley, J. S. 1932. Problems of Relative Growth. Methuen & Co. Ltd., London, UK.

Johnson, M. D., J. Völker, H. V. Moeller, E. Laws, K. J. Breslauer, and P. G. Falkowski. 2009. Universal constant for heat production in protists. Proc. Natl. Acad. Sci. USA 106: 6696-6699.

Kempes, C. P., S. Dutkiewicz, and M. J. Follows. 2012. Growth, metabolic partitioning, and the size of microorganisms. Proc. Natl. Acad. Sci. USA 109: 495-500.

Kimura, M., T. Maruyama, and J. F. Crow. 1963. The mutation load in small populations. Genetics 48: 1303-1312.

Kleiber, M. 1932. Body size and metabolism. Hilgardia 6: 315-353.

Kleiber, M. 1947. Body size and metabolic rate. Physiol. Rev. 27: 511-541.

Kozłowski, J., and M. Konarzewski. 2004. Is West, Brown and Enquist's model of allometric scaling mathematically correct and biologically relevant? Func. Ecol. 18: 283-289.

Kozłowski, J., and M. Konarzewski. 2005. West, Brown and Enquist's model of allometric scaling again: the same questions remain. Func. Ecol. 19: 739-743.

Kühlbrandt, W. 2015. Structure and function of mitochondrial membrane protein complexes. BMC Biol. 13: 89.

Lane, N. 2002. Power, Sex, Suicide: Mitochondria and the Meaning of Life. Oxford Univ. Press, Oxford, UK.

Lane, N. 2015. The Vital Question. W. W. Norton & Co., Inc. New York, NY.

Lane N. 2020. How energy flow shapes cell evolution. Curr. Biol. 30: R471-R476.

Lane, N., and W. Martin. 2010. The energetics of genome complexity. Nature 467: 929-934.

Lennon, J. T., F. den Hollander, M. Wilke-Berenguer, and J. Blath. 2021. Principles of seed banks and the emergence of complexity from dormancy. Nat. Commun. 12: 4807.

Lücken, U., E. P. Gogol, and R. A. Capaldi. 1990. Structure of the ATP synthase complex (ECF1F0) of *Escherichia coli* from cryoelectron microscopy. Biochem. 29: 5339-5343.

Lynch, M. 2020. The evolutionary scaling of cellular traits imposed by the drift barrier. Proc. Natl. Acad. Sci. USA 117: 10435-10444.

Lynch, M., and G. K. Marinov. 2015. The bioenergetic costs of a gene. Proc. Natl. Acad. Sci. USA 112: 15690-15695.

Lynch, M., and G. K. Marinov. 2017. Membranes, energetics, and evolution across the prokaryote-eukaryote divide. eLife 6: e20437.

Lynch, M., and G. K. Marinov. 2018. Reply to Martin and colleagues: mitochondria do not boost the bioenergetic capacity of eukaryotic cells. Biology Direct 13: 26.

Lynch, M., P. E. Schavemaker, T. J. Licknack, Y. Hao, and A. Pezzano. 2022a. Evolutionary bioenergetics of ciliates. J. Euk. Microbiol. (in press).

Lynch, M., B. Trickovic, and C. P. Kempes. 2022b. Evolutionary scaling of maximum growth rates with cell size. Sci. Reports (in revision).

Lynch, M., and J. B. Walsh. 1998. Genetics and Analysis of Quantitative Traits. Sinauer Assocs., Inc., Sunderland, MA.

Magalon, A., and F. Alberge. 2015. Distribution and dynamics of OXPHOS complexes in the bacterial cytoplasmic membrane. Biochim. Biophys. Acta 1857: 198-213.

Marañòn, E. 2015. Cell size as a key determinant of phytoplankton metabolism and community structure. Annu. Rev. Mar. Sci. 7: 241-264.

Marañón, E, P. Cermeño, D. C. López-Sandoval, T. Rodriguez-Ramos, C. Sobrino, M. Huete-Ortega, J. M. Blanco, and J. Rodriguez. 2013. Unimodal size scaling of phytoplankton growth and the size dependence of nutrient uptake and use. Ecol. Lett. 16: 371-379.

Marshall, W. F. 2020. Scaling of subcellular structures. Annu. Rev. Cell Dev. Biol. 36: 219-236.

Milo, R., and R. Phillips. 2016. Cell Biology by the Numbers. Garland Science, Taylor & Francis Group, New York, NY.

Mookerjee, S. A., A. A. Gerencser, D. G. Nicholls, and M. D. Brand. 2017. Quantifying intracellular rates of glycolytic and oxidative ATP production and consumption using extracellular flux measurements. J. Biol. Chem. 292: 7189-7207.

Morono, Y., M. Ito, T. Hoshino, T. Terada, T. Hori, M. Ikehara, S. D'Hondt, and F. Inagaki F. 2020. Aerobic microbial life persists in oxic marine sediment as old as 101.5 million years. Nat. Commun. 11: 3626.

Munder, M. C., D. Midtvedt, T. Franzmann, E. Nüske, O. Otto, M. Herbig, E. Ulbricht, P. Müller, A. Taubenberger, S. Maharana, et al. 2016. A pH-driven transition of the cytoplasm from a fluid- to a solid-like state promotes entry into dormancy. eLife 5: e09347.

Okie, J. G. 2013. General models for the spectra of surface area scaling strategies of cells and organisms: fractality, geometric dissimilitude, and internalization. Am. Nat. 181: 421-439.

Osafune, T., S. Mihara, E. Hase, and I. Ohkuro. 1975. Electron microscope studies of the vegetative cellular life cycle of *Chlamydomonas reinhardi* Dangeard in synchronous culture. III. Three-dimensional structures of mitochondria in the cells at intermediate stages of the growth phase of the cell cycle. J. Electron Microsc. (Tokyo) 24: 247-252.

Pellegrini, M. 1980. Three-dimensional reconstruction of organelles in *Euglena gracilis* Z. I. Qualitative and quantitative changes of chloroplasts and mitochondrial reticulum in synchronous photoautotrophic culture. J. Cell Sci. 43: 137-166.

Pirt, S. J. 1982. Maintenance energy: a general model for energy-limited and energy-sufficient growth. Arch. Microbiol. 133: 300-302.

Pittis, A. A., and T. Gabaldón. 2016 Late acquisition of mitochondria by a host with chimaeric prokaryotic ancestry. Nature 531: 101-104.

Posakony, J. W., J. M. England, and G. Attardi. 1977. Mitochondrial growth and division during the cell cycle in HeLa cells. J. Cell Biol. 74: 468-491.

Rafelski, S. M., M. P. Viana, Y. Zhang, Y. H. Chan, K. S. Thorn, P. Yam, J. C. Fung, H. Li, F. Costa Lda, and W. F. Marshall. 2012. Mitochondrial network size scaling in budding yeast. Science 338: 822-824.

Raven, J. A. 1986. Physiological consequences of extremely small size for autotrophic organisms in the sea, pp. 1-70. *In* T. Platt and E. K. W. Li (eds.) Photosynthetic picoplankton. Can. Bull. Fish. Oceans.

Raven, J. A. 1994. Why are there no picoplanktonic O2 evolvers with volumes less than 10^{-19} m^3? J. Plank. Res. 16: 565-580.

Rosen, D., M. Edelman, E. Galun, and D. Danon. 1974. Biogenesis of mitochondria in *Trichoderma viride:* structural changes in mitochondria and other spore constituents during conidium maturation and germination. Microbiol. 83: 31-49.

Russell, J. B., and G. M. Cook. 1995. Energetics of bacterial growth: balance of anabolic and catabolic reactions. Microbiol. Rev. 59: 48-62.

Savage, V. M., B. J. Enquist, and G. B. West. 2007. Comment on 'A critical understanding of the fractal model of metabolic scaling'. J. Exp. Biol. 210: 3873-3874.

Stock, D., A. G. Leslie, and J. E. Walker. 1999. Molecular architecture of the rotary motor in ATP synthase. Science 286: 1700-1705.

Tarkington, J., and R. A. Zufall. 2021. Temperature affects the repeatability of evolution in the microbial eukaryote *Tetrahymena thermophila*. Ecol. Evol. 11: 13139-13152.

Tempest, D. W., and O. M. Neijssel. 1984. The status of YATP and maintenance energy as biologically interpretable phenomena. Annu. Rev. Microbiol. 38: 459-486.

Thompson, D. A. 1917. On Growth and Form. Cambridge Univ. Press, Cambridge, UK.

Tyn, M. T., and T. W. Gusek. 1990. Prediction of diffusion coefficients of proteins. Biotechnol. Bioeng. 35: 327-338.

Uwizeye, C., J. Decelle, P.-H. Jouneau, S. Flori, B. Gallet, J.-B. Keck, D. Dal Bo, C. Moriscot, C. Seydoux, F. Chevalier, et al. 2021. Morphological bases of phytoplankton energy management and physiological responses unveiled by 3D subcellular imaging. Nat. Comm. 12: 1049.

van Bodegom, P. 2007. Microbial maintenance: a critical review on its quantification. Microb. Ecol. 53: 513-523.

von Bertalanffy, L. 1957. Quantitative laws in metabolism and growth. Quart. Rev. Biol. 32: 217-231.

Ward, B. A., E. Marañòn, B. Sauterey, J. Rault, and D. Claessen. 2017. The size dependence of phytoplankton growth rates: a trade-off between nutrient uptake and metabolism. Am. Nat. 189: 170-177.

West, G. 2017. Scale: the Universal Laws of Growth, Innovation, Sustainability, and the Pace of Life in Organisms, Cities, Economies, and Companies. Penguin Press, London, UK.

West, G. B., J. H. Brown, and B. J. Enquist. 1997. A general model for the origin of allometric scaling laws in biology. Science 276: 122-126.

West, G. B., J. H. Brown, and B. J. Enquist. 1999. The fourth dimension of life: fractal geometry and allometric scaling of organisms. Science 284: 1677-1679.

West, G. B., W. H. Woodruff, and J. H. Brown. 2002. Allometric scaling of metabolic rate from molecules and mitochondria to cells and mammals. Proc. Natl. Acad. Sci. USA 99 Suppl. 1: 2473-2478.

Wieser, W. 1994. Cost of growth in cells and organisms: general rules and comparative aspects. Biol. Rev. 69: 1-33.

Wiser, M. J., N. Ribeck, and R. E. Lenski. 2013. Long-term dynamics of adaptation in asexual populations. Science 342: 1364-1367.

Yamaguchi, M., Y. Namiki, H. Okada, Y. Mori, H. Furukawa, J. Wang, M. Ohkusu, and S. Kawamoto. 2011. Structome of *Saccharomyces cerevisiae* determined by freeze-substitution and serial ultrathin-sectioning electron microscopy. J. Electron Microsc. (Tokyo) 60: 321-335.

Zeuthen, E. 1953. Oxygen uptake as related to body size in organisms. Quart. Rev. Biol. 28: 1-12.

Figure 8.1. Distributions of species-specific cell volumes for major phylogenetic groups for which multiple measures are available. Solid points denote group means, bold and narrow horizontal bars denote standard deviations and ranges. Data from Lynch et al. (2022b).

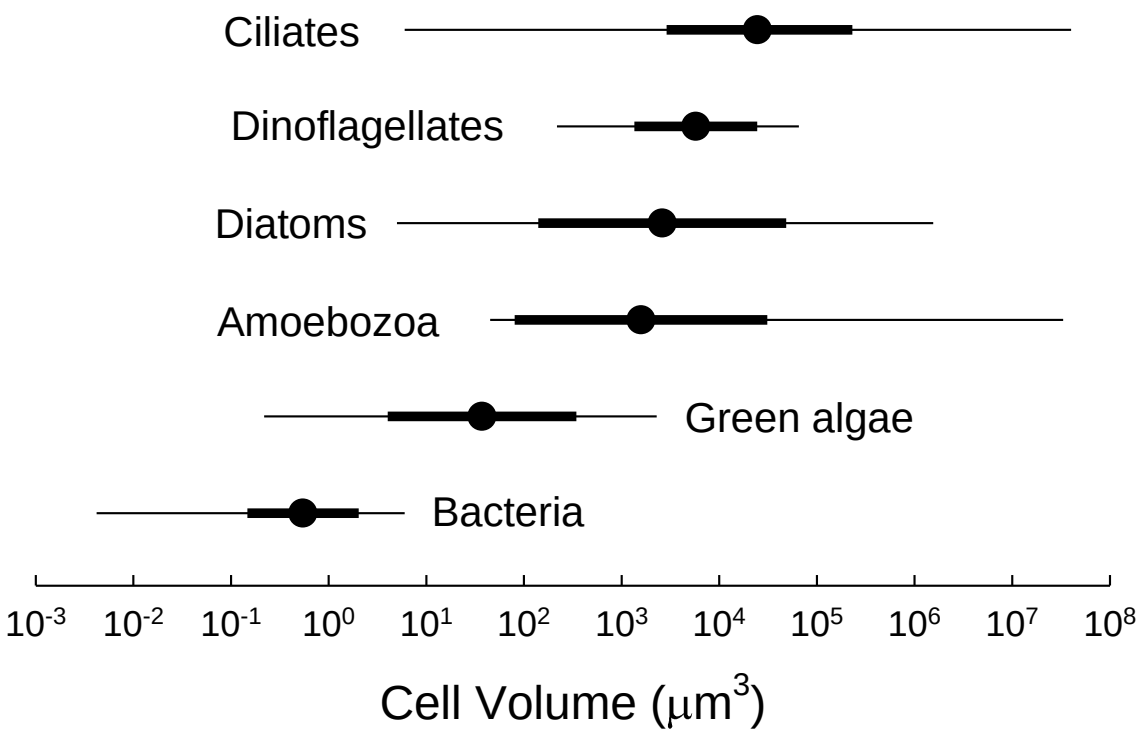

Figure 8.2. Allometric scalings of metabolic rate per cell (M) with cell volume (V) in heterotrophic unicellular species, with units given on the axes: $M = 23.3B^{1.01}$ (solid black line; standard error of exponent = 0.03); separate regressions for bacteria and unicellular eukaryotes (dashed lines) have slopes of 1.26 and 0.97, respectively, although these are not significantly different. Data are from DeLong et al. (2010) with updated cell volumes derived from the survey in Lynch et al. (2022b). All metabolic rates are scaled to expected values at 20°C using a Q_{10} value of 2.5.

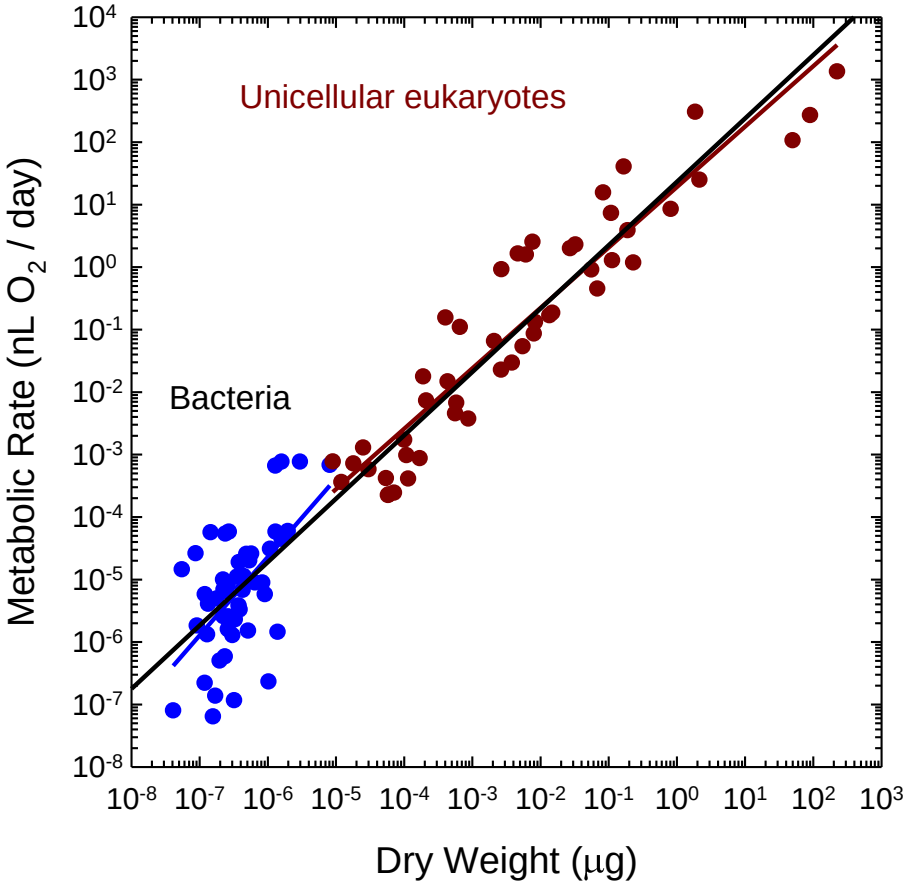

Figure 8.3. Estimating the costs of building and maintaining cells with chemostat cultures. **Left**) A chemostat (the central vessel) with a continuous input of resources (set by the valve on the upper reservoir containing sterile medium) and outflow into the bottom discard container. Aeration ensures an even distribution of cells within the culture and helps prevent wall growth. **Right**) A typical Pirt plot of the rate of glucose consumption by cultures of a bacterium grown at different dilution rates. Note that the measure of resource consumption is in units of glucose / total cell dry weight; this can be converted to ATP consumption per cell using information on the ATP equivalents derived per unit glucose consumed and the dry weight of individual cells. The y-intercept, with units of resource consumed / cell dry weight / time, is a measure of the basal maintenance requirement; the slope, with units of resource consumed / cell division (beyond basal metabolic requirements), is a measure of the total resource requirements for cell growth.

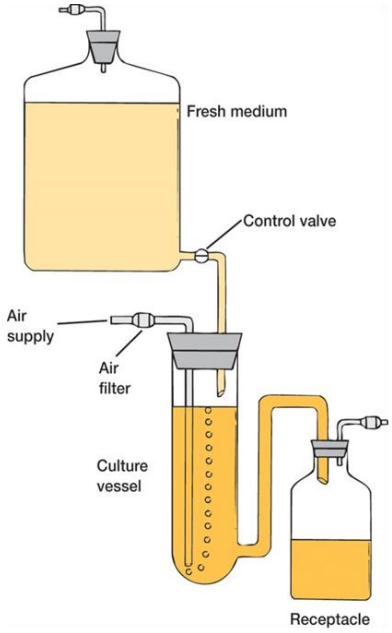

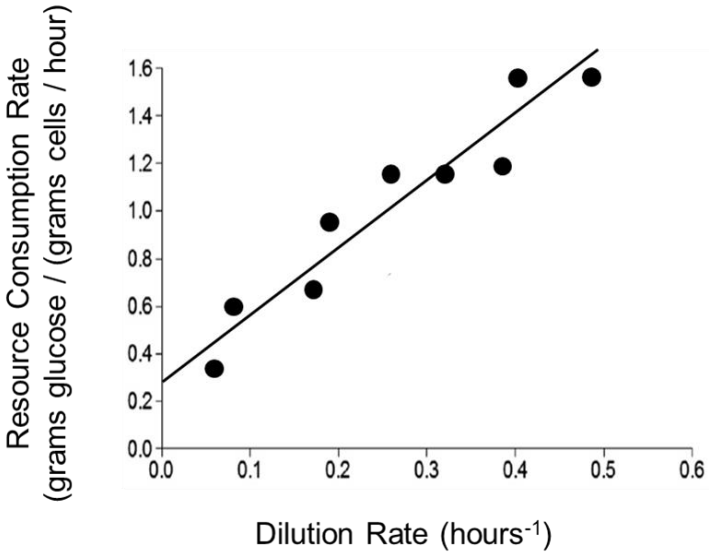

Figure 8.4. Cellular energetic requirements in units of numbers of ATP → ADP hydrolysis events, all scaled to 20°C to normalize results from studies involving different temperatures. The maintenance and growth costs for bacterial (black) and unicellular eukaryotic (blue) species are fitted together with allometric regression lines. Growth data for cell cultures from a few multicellular eukaryotes (red) are not included in the regression analysis. From Lynch and Marinov (2015).

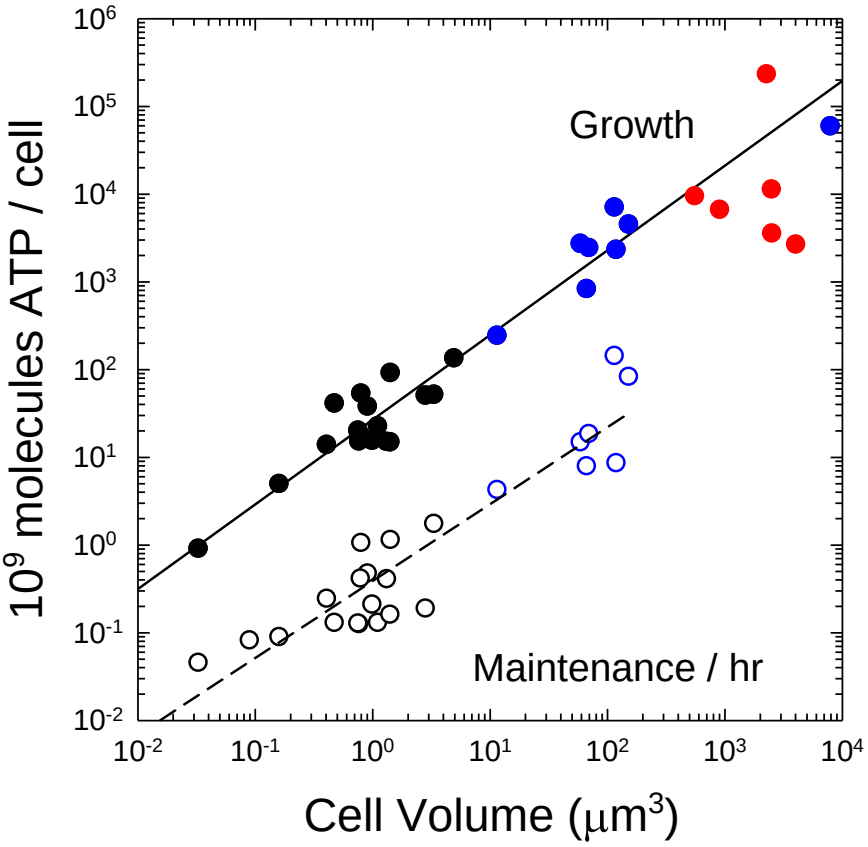

Figure 8.5. Maximum growth rates, $\ln(2)$/doubling time, for a) heterotrophic and b) phototrophic unicellular species, scaled to expected values at 20°C. Fitted lines are given only for the cases in which the least-squares regression is significant; the slopes are 0.28 for heterotrophic bacteria, -0.21 for amoeboid eukaryotes, -0.22 for ciliates, -0.21 for heterotrophic flagellates (excluding dinoflagellates), -0.19 for dinoflagellates, and -0.09 for both green algae and diatoms. The dashed ellipses enveloping the data for bacterial and eukaryotic heterotrophs in the upper panel are transferred to the lower panel for comparative purposes. From Lynch et al. (2022a).

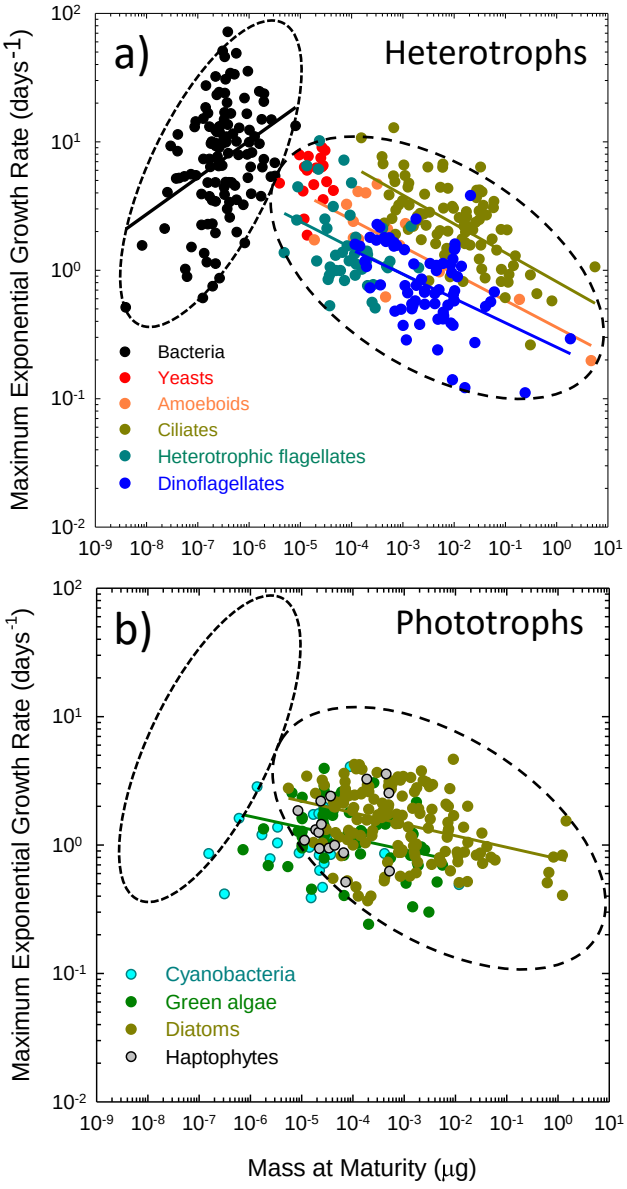

Figure 8.6. Evolutionary long-term average performance (under drift-mutation-selection balance) relative to the maximum value of a trait experiencing an exponential fitness function. Each locus has two possible alleles, + and −, with additive effects on the trait, but with individual fitness declining as e^{-sn}, where s is the selective disadvantage, and n is the number of − alleles per individual. Reversible mutation operates between the two alternative alleles at rates u_{01} from − to +, and u_{10} from + to −. Populations consist of N haploid individuals. **a)** Results are given for four values of s for the situation in which there is free recombination between sites. Mean performance makes a rapid transition from the neutral expectation $u_{01}/(u_{01}+u_{10})$ to the domain in which the beneficial-allele frequency $\simeq 1$ at the point at which $1/N = s$. Analytical results are obtained from formulae in Kimura et al. (1963). **b)** Results for the situation in which $s = 10^{-6}$, under the assumption of L completely linked genomic sites, all with the same effects. With larger numbers of linked sites, the gradient in mean performance with N becomes more gradual. Here and in panel **d**, the results are obtained by computer simulation using the methods in Lynch (2020). **c)** Modification of the situation in panel **a** to allow for a mixture of unlinked genomic sites with different effects, with various weights given to the four curves in panel **a**. As the population size increases, selection becomes progressively more efficient at promoting alleles with smaller effects. For example, $L = 10\times$ means that for each site with effect $s = 10^{-5}$, there are ten with $s = 10^{-6}$, 100 with $s = 10^{-7}$, and 1000 with $s = 10^{-8}$. **d)** The situation in which there are blocks of linked loci, one major-effect site with $s = 10^{-5}$, and variable numbers (L) of linked loci with minor effects $s = 10^{-7}$. As L increases, the minor loci contribute proportionally more to total performance, and create background selection interference with the major locus and amongst themselves.

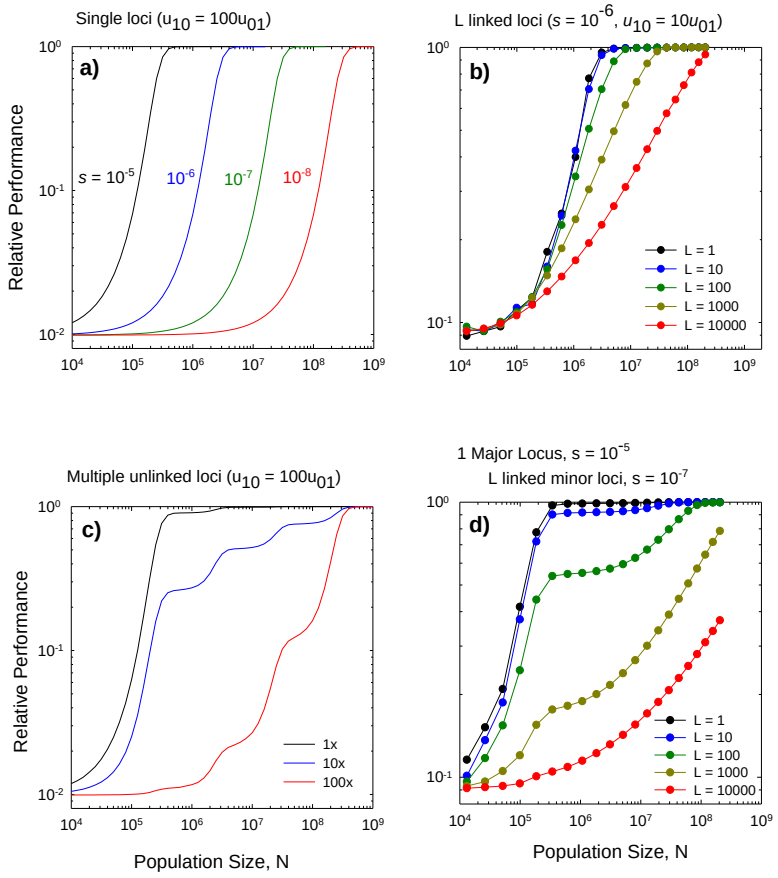

Figure 8.7. The scaling of mitochondrial features with cell size. **Left**) Relationship between the total outer surface area of mitochondria and that of the plasma membrane. Diagonal lines denote three idealized ratios of the two. Data are from Lynch and Marinov (2017) and Uwizeye et al. (2021). **Right**) The number of ATP synthase complexes per cell scales with cell surface area (S, in μm^2) as $113S^{1.26}$ ($r^2 = 0.99$); black data points are for bacteria.

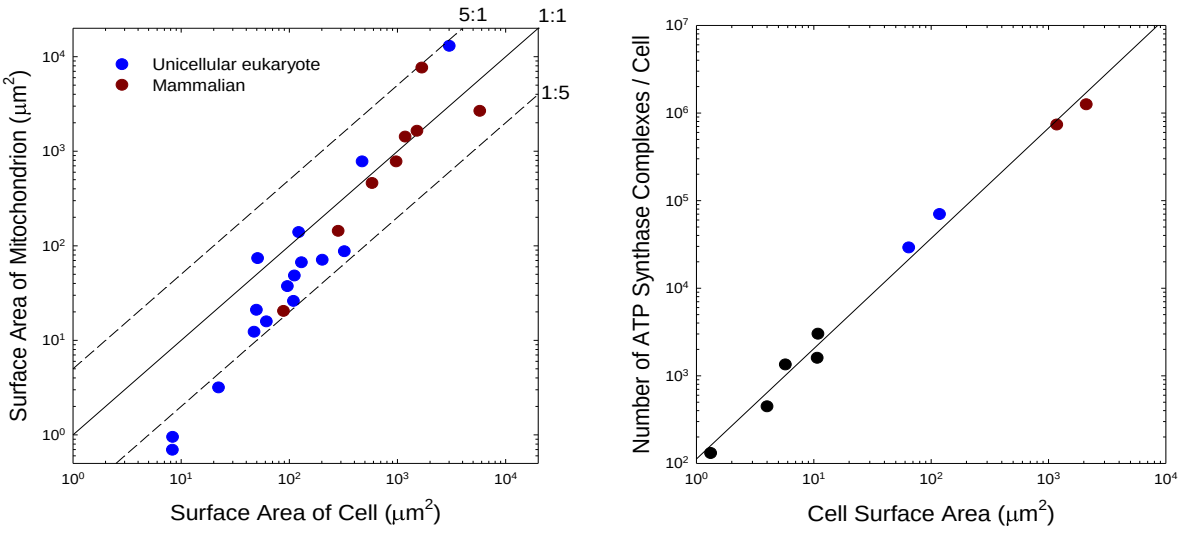

Figure 8.8. The number of ribosomes per cell scales with cell volume (V, in μm^3) as $8810V^{0.80}$ ($r^2 = 0.92$; standard error of the exponent = 0.04). Color coding as in the previous figure, with green denoting green algae and land-plant cells. From Lynch and Marinov (2017, 2018) and a few additional data points from more recent literature (Supplemental Table 8.3). Although the estimated slope based on bacterial data alone is hypermetric, and that for eukaryotes alone is hypometric, neither is significantly different from 1.0, nor from each other.

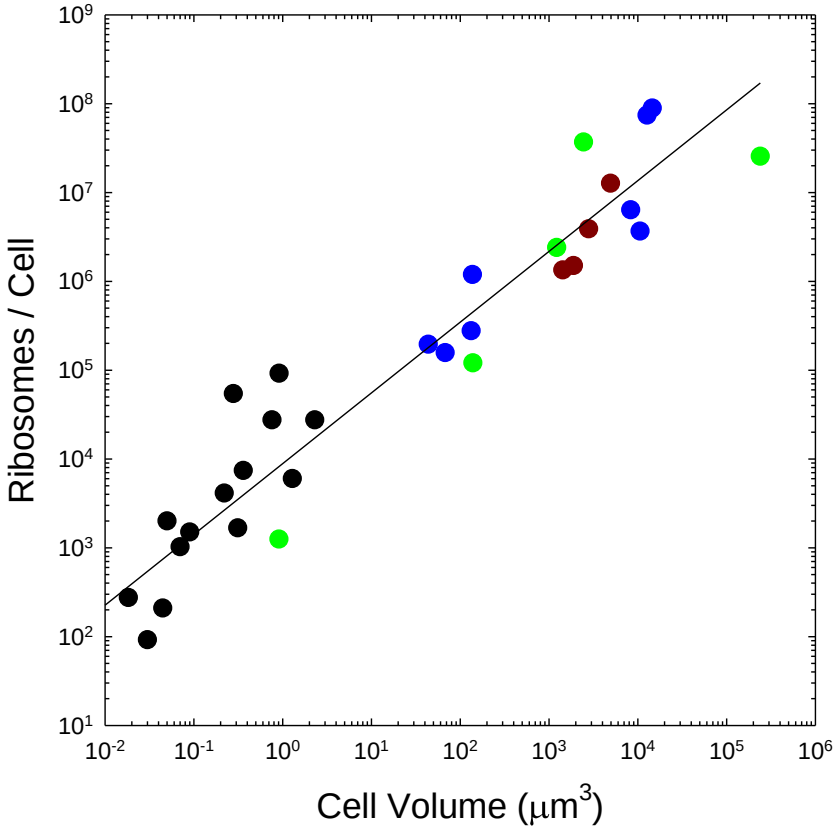

Figure 8.9. Allometric regressions of maximum growth rate and metabolic rates of ciliates, with all values normalized to a temperature of 20° C. From Lynch et al. (2022b).